# Open Archive Toulouse Archive Ouverte (OATAO)

Any correspondence concerning this service should be sent to the repository administrator: tech-oatao@listes-diff.inp-toulouse.fr

# A Generic Method of Pulsewidth Modulation Applied to Three-Phase Three-Level T-Type NPC Inverter

Simon Cailhol, Paul-Etienne Vidal, and Frédéric Rotella, *Senior Member, IEEE*

*Abstract*—This paper illustrates the application of a solving method of linear systems to a multilevel inverter. This study applies a generic pulsewidth modulation (PWM) method to a multilevel topology. This method finally highlights some specific modulation schemes. First, the study describes the mathematical model of the inverter leg. The leg is made of three level T-type structure. The model is extended to the three-phase inverter. The generalized inverse is used to generate the solution set of the conduction rates. Among the modulation strategies possible, three specific modulation schemes are proposed. The modulation schemes are applied to simulate a PWM three-phase inverter. Finally, some experimental results complete the analysis.

*Index Terms*—Circuit modeling, dc–ac power conversion, energy conversion, pulsewidth modulation (PWM), pulsewidth modulated inverters.

## I. INTRODUCTION

**E**LECTRIFIED systems are of growing importance in many applications developed today. Among them, some widespread applications such as pipeline pumps [1], fans [2], water pumping stations [3], and traction applications [4] concern medium voltage converters. New trends for converter design, emerging from eco-friendly applications, are commonly studied. Grid integration of renewable-energy sources [5], reactive-power compensation [6] in order to maximize the system efficiency and so on, belong to this category. It is noted that for such applications, the converter control achieves the exchanged energy monitoring. Consequently, the converter architecture and its control are the key issues for the electric power conversion applications.

The availability of widebandgap semiconductors, combined with their increase reliability leads to new interest for developing original inverter topologies. Indeed, studies work on the correlation of a given architecture and its dedicated modulation strategy with an application. Among these studies, the multilevels architecture and particularly the neutral point clamped (NPC) were widely studied. First, dedicated to high power application, a de-

rived topology, named three level T-type converter ($3LT^2C$) is under interest. Effectively, this topology benefits from its ability at being used in high power photovoltaic systems [7], as well as variable speed drives for low voltages applications, [8]. Moreover, it has been demonstrated that a $3LT^2C$ increases the converter efficiency compared to similar multilevel inverters, and more precisely compared to a three-level NPC, with respect to power losses [9], [13].

Studies demonstrated that the modulation strategy of a three-level NPC can also be applied to the $3LT^2C$ topology. Indeed, usual carrier based pulsewidth modulation (PWM) associated with two carrier waveforms [10], or space vector modulation (SVM) which allows harmonic selection [11], have been successfully tested. Nevertheless, the major drawbacks of such an inverter topology concern the control of the common mode voltage or the unbalance voltage of dc input sources. Most of the modulation strategies aim to balance these drawbacks.

It appears to our knowledge that it does not exist any generic modulation model of $3LT^2C$ converter. The aim of this study is to apply the PWM modeling technique proposed in [12], in order to establish a generic inverter modulation model of such a structure, which can match the following criteria:

1) to be applied to carrier-based PWM;
2) to be extended to SVM principles;
3) to highlight how to implement a generic modulation scheme;
4) to define admissible modulation solutions.

The contribution of this paper is twofold, which is given as follows:

1) the modeling of the T-type $3LT^2C$ converter in a generic framework;
2) the determination of modulation strategies using a generic mathematical method.

This paper is organized as follows: first, the considered structure is described and a mathematical model is proposed in Section II. Then, based on the defined model, the considerations to generate modulation strategies are provided. Three modulation strategies are described in Section III. Simulation results are provided in Section IV-C. Finally, some experimental results allow us to recover the theoretical and simulation data. A discussion section analyze the efficiency of the generic model as well as its ability to produce the efficient PWM schemes.

## II. INVERTER MODELING

From a practical point of view, a three-phase $3LT^2C$ inverter is made of three legs based on a similar switching cell structure.

*(Corresponding author: Simon Cailhol.)*

The authors are with the Laboratoire Génie de Production, Université Fédérale de Toulouse, Tarbes Cedex 65016, France (e-mail: simon.cailhol@enit.fr; paul-etienne.vidal@enit.fr; frotella@enit.fr).

Color versions of one or more of the figures in this paper are available online at http://ieeexplore.ieee.org.
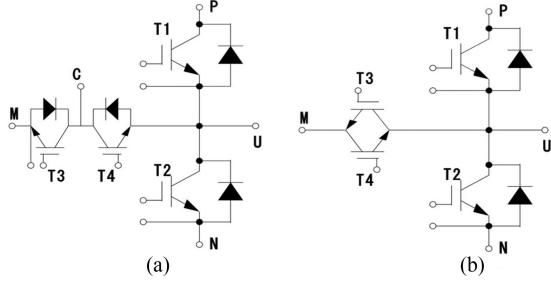
Fig. 1. T-type switching cells [14]. (a) Normal. (b) RB-IGBT based.

TABLE I
OUTPUT VOLTAGES

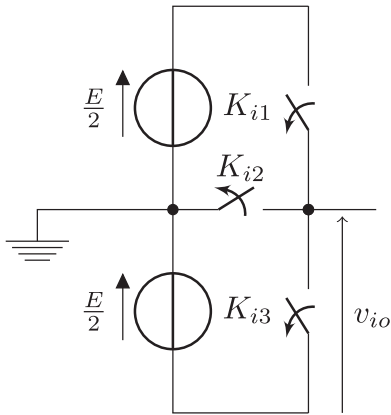| $K_{i1}$ | $K_{i2}$ | $K_{i3}$ | $v_{io}$ |
|---|---|---|---|
| 1 | 0 | 0 | $E$ |
| 0 | 1 | 0 | $\dfrac{E}{2}$ |
| 0 | 0 | 1 | 0 |



Fig. 2. Elementary cell structure.

In this section, we will first detail the model of a leg of such an inverter and then extend this model to a complete three-phase inverter.

### A. T-Type Switching Cell

The switching cell can be built from two technological achievements, as illustrated in Fig. 1. This figure depicts the electrical equivalent circuits of available commercial modules. The inverter cell of the leg $i$ considered is made of three switches, named $K_{i1}$, $K_{i2}$, and $K_{i3}$. Due to the switches connection, to avoid short circuit of the input voltage sources, only one switch can be turned ON at once. Thus, $K_{i1}$, $K_{i2}$, and $K_{i3}$ are elementary switching cells. Every switch state corresponds to an output line voltage $v_{io}$, as given in Table I. The other possibilities are not allowed.

As far as the modulation model is concerned, the switching cell can be considered as three elementary ideal switches, associated with two independent and perfect input voltage sources, as illustrated in Fig. 2.

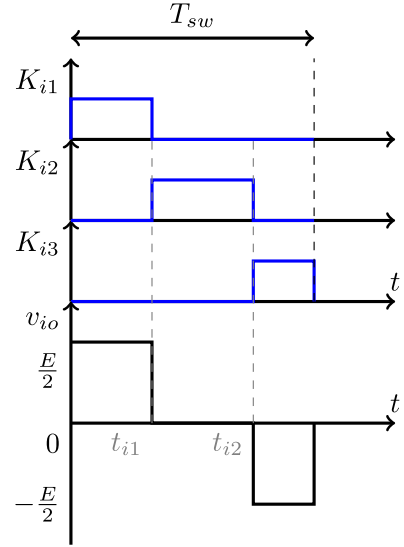The Fig. 3 gives an example of a switching sequence and the corresponding line voltage during the period $T_{\text{sw}}$, where



Fig. 3. Example of a switching sequence.

$f_{\text{sw}} = \dfrac{1}{T_{\text{sw}}}$ is the switching frequency. In such example, it is assumed that every switch can be turned ON and OFF at every $T_{\text{sw}}$.

As exemplified in Fig. 3, $t_{i1}$ is the time when $K_{i1}$ is closed. Then, $K_{i2}$ is switched ON from $t_{i1}$ to $t_{i2}$, and finally $K_{i3}$ between $t_{i2}$ and $T_{\text{sw}}$. To recover the carrier-based PWM schemes, let us define, $\tau_{i,k}$, $k \in \{1; 2; 3\}$ as the conduction rates, or duty cycles, of switch $K_{ik}$ over $T_{\text{sw}}$

$$\tau_{i1} = \frac{t_{i1}}{T_{\text{sw}}}$$

$$\tau_{i2} = \frac{t_{i2} - t_{i1}}{T_{\text{sw}}}$$

$$\tau_{i3} = \frac{T_{\text{sw}} - t_{i2}}{T_{\text{sw}}} . \tag{1}$$

The mean value of the line voltage over the switching period, $V_{io}$, is computed as

$$V_{io} = \frac{E}{2} \left( \tau_{i1} - \tau_{i3} \right). \tag{2}$$

Unfortunately, these conduction rates, associated with a carrier-based PWM scheme, does not allow us to produce the line voltage depicted in Fig. 3. Then, new variables are defined. As $K_{i3}$ state is dependent of $K_{i1}$ and $K_{i2}$ states, let us express $a_{i1}$ and $a_{i2}$ as a function of the switching times $t_{i1}$ and $t_{i2}$ as

$$\begin{cases} a_{i1} & = \dfrac{t_{i1}}{T_{\text{sw}}} \\ a_{i2} & = \dfrac{t_{i2}}{T_{\text{sw}}} . \end{cases} \tag{3}$$

As illustrated in Fig. 4, an advantage of such a model appears: a carrier-based modulation scheme is used, associated with a single carrier easily generated. Finally, the switching times $t_{i1}$ and $t_{i2}$ are used to generate every control signal for $K_{ik}$. They are obtained, thanks to the Boolean function of the comparison of $a_i$ to a sawtooth signal defined between 0 and 1 at frequency $f_{\text{sw}}$, as illustrated in Fig. 4.
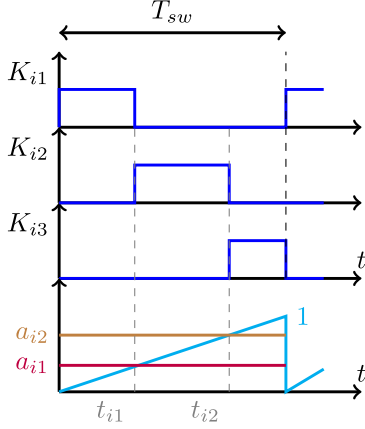
Fig. 4.    Command orders generation principle.

Finally, the mean value of the line voltage, $V_{io}$, is deduced

$$V_{io} = \frac{E}{2}\left(a_{i1} + a_{i2}\right) - \frac{E}{2}. \tag{4}$$

Defining $V_{io}^* = V_{io} + \frac{E}{2}$ leads to the relationship

$$V_{io}^* = \frac{E}{2}Aa_i \quad \forall i, \, i \in \{1,2,3\} \tag{5}$$

where $A = \begin{bmatrix} 1 & 1 \end{bmatrix}$ and $a_i = \begin{bmatrix} a_{i1} & a_{i2} \end{bmatrix}^T$. The control strategy vector $a_i$ appears as the solution of the linear system (5).

### B.  $3LT^2C$ Inverter

The model of the three-phase inverter is obtained by duplicating (5), thanks to the Kronecker product $\otimes$

$$V_{lo}^* = \frac{E}{2}\left(I_3 \otimes A\right)a \tag{6}$$

where $V_{lo}^*$ is the vector of the three line voltages $V_{io}^*$ such as $V_{lo}^* = \begin{bmatrix} V_{1o}^* & V_{2o}^* & V_{3o}^* \end{bmatrix}^T$ and $a = \begin{bmatrix} a_1 & a_2 & a_3 \end{bmatrix}^T$. $I_3$ is the $3 \times 3$ identity matrix.

The Kronecker product $\otimes$ performs a weighted duplication of the matrix $A$ on each component of $I_3$ [15], [16].

With a three-phase balanced load, the phase voltage vector $V_{ln}$ is

$$V_{ln} = MV_{lo} \tag{7}$$

where $M$ is defined

$$M = \frac{1}{3}\begin{bmatrix} 2 & -1 & -1 \\ -1 & 2 & -1 \\ -1 & -1 & 2 \end{bmatrix}.$$

Moreover, the neutral point voltage introduced for the phase voltage calculation allows simplifying $V_{ln}$ such as

$$V_{ln} = MV_{lo} = MV_{lo}^*. \tag{8}$$

Due to $M(I_3 \otimes A) = M \otimes A$ and [17], the inverter model can be expressed as a linear problem

$$V_{ln} = \frac{E}{2}\left(M \otimes A\right)a \tag{9}$$

where the unknown are the $a_{ij}$.

## III.  Control Strategies

For an elementary switching cell, the solution expressions were expressed and detailed in [18]. The aim of the following section is to extend these methods to a three-phase inverter.

### A.  Generic Solutions

Let us observe that $\mathrm{rank}(M \otimes A) = \mathrm{rank}\left(\begin{bmatrix} M \otimes A & V_{ln} \end{bmatrix}\right)$ is fulfilled for the sake of necessity. Thus, the linear system (9) is consistent. The solutions are using $(M \otimes A)^\dagger$, which is the pseudoinverse of $(M \otimes A)$ [19]

$$a = \frac{2}{E}(M \otimes A)^\dagger V^{\mathrm{ref}} + \left(I_6 - (M \otimes A)^\dagger(M \otimes A)\right)z \tag{10}$$

where $z$ is an arbitrary six-dimensional vector.

Then, the solutions are split in two summed up parts as follows.
1) A fixed solution: $\frac{2}{E}(M \otimes A)^\dagger V^{\mathrm{ref}}$, which is noted $a^{\mathrm{ref}}$.
2) An independent solution: $\left(I_6 - (M \otimes A)^\dagger(M \otimes A)\right)z$, which is in the kernel of $M \otimes A$.

Looking at the independent solution, some degrees of freedom can be deduced from $(I_6 - (M \otimes A)^\dagger(M \otimes A))z$. The degree of freedom $n_\lambda$, which is the dimension of the kernel of $M \otimes A$, is given by

$$n_\lambda = n - \mathrm{rank}(M \otimes A) = 4 \tag{11}$$

where $n$ is the number of columns of $M \otimes A$.

A simple way to exhibit a $n_\lambda$-dimensional vector $\lambda$ is to use a maximal rank factorization algorithm. Namely there exists $F$, a full column rank $(n \times n_\lambda)$-dimensional matrix and $G$, a full row rank $(n_\lambda \times n)$-dimensional matrix, such as

$$FG = I_6 - (M \otimes A)^\dagger(M \otimes A). \tag{12}$$

Defining $\lambda = Gz$, the control vector $a$ is obtained

$$a = (M \otimes A)^\dagger V^{\mathrm{ref}} + F\lambda = a^{\mathrm{ref}} + F\lambda \tag{13}$$

where $\lambda = \begin{bmatrix} \lambda_1 & \lambda_2 & \lambda_3 & \lambda_4 \end{bmatrix}$ is the tuning parameters vector.

The matrix $F$ is chosen in order to ease the tuning parameters manipulation (see the Appendix)

$$F = \begin{bmatrix} -1 & 0 & 0 & 1 \\ 1 & 0 & 0 & 1 \\ 0 & -1 & 0 & 1 \\ 0 & 1 & 0 & 1 \\ 0 & 0 & -1 & 1 \\ 0 & 0 & 1 & 1 \end{bmatrix}. \tag{14}$$

Furthermore, the line voltage $V_{io}$ defined in (4) combined with the expression of $a$ in (13) allows us to compute the neutral point voltage $V_{no}$ as

$$V_{no} = E\lambda_4 - \frac{E}{2}. \tag{15}$$

Therefore, $\lambda_4$ appears as the common mode tuning parameter, whereas $\lambda_1$, $\lambda_2$, and $\lambda_3$ are legs tuning parameters.

## B. Implementation Constraints

Among the solution set expressed in (13), some solutions are not physically acceptable. Indeed, components of $a$ have to be in $[0, 1]$. Moreover, among each inverter leg, they have to be ordered. These two constraints are summarized as

$$0 \leq a_{ij} \leq 1 \tag{16}$$

$$a_{i1} \leq a_{i2}. \tag{17}$$

Due to the structure of the matrix $(M \otimes A)^\dagger$, the fixed elements $a_{i1}^{\text{ref}}$ and $a_{i2}^{\text{ref}}$ of the solution are equal and are denoted a $a_i^{\text{ref}}$.

Considering the independent solution, two aspects of the tuning parameters can be stated as follows.

*1) Common Mode Tuning Parameter:* $\lambda_4$ acts on every element of the vector $a$. Thus, it must be tuned first according to (16). Indeed, $0 \leq a_{ij} \leq 1$, $i \in \{1, 2, 3\}$, $j \in \{1, 2\}$ leads to $0 \leq a_i^{\text{ref}} + \lambda_4 \leq 1$ which defines bounds for $\lambda_4$

$$-\min(a^{\text{ref}}) \leq \lambda_4 \leq 1 - \max(a^{\text{ref}}). \tag{18}$$

These bounds will be denoted by $\lambda_{4_{\text{low}}}$ and $\lambda_{4_{\text{high}}}$ in the following.

*2) Per Leg Tuning Parameter:* The $\lambda_i$ $i \in \{1, 2, 3\}$ are dedicated to phases $i$, respectively. Once $\lambda_4$ is defined, the other components of $\lambda$ are set accordingly to (16) and (17).

First, (17) leads to

$$\lambda_i \geq 0. \tag{19}$$

Second, (16) can be split in two parts.
1) A lower bound

$$\lambda_i \leq a_i^{\text{ref}} + \lambda_4. \tag{20}$$

2) A upper bound inequality

$$\lambda_i \leq 1 - (a_i^{\text{ref}} + \lambda_4). \tag{21}$$

Finally, for $\lambda_i$ $i \in \{1, 2, 3\}$, the three conditions (19)–(21) are summed up as

$$0 \leq \lambda_i \leq \min(a_i^{\text{ref}} + \lambda_4, 1 - (a_i^{\text{ref}} + \lambda_4)). \tag{22}$$

The upper bound appearing in (22) will be denoted as $\lambda_{i_{\text{high}}}$ for $i \in \{1, 2, 3\}$.

## IV. PARTICULAR SOLUTIONS

### A. Common Mode Tuning Parameter

In this study, the common mode tuning parameter $\lambda_4$ is chosen at the middle point, namely

$$\begin{aligned} \lambda_4 &= \frac{\lambda_{4_{\text{low}}} + \lambda_{4_{\text{high}}}}{2} \\ &= \frac{-\min(a_i^{\text{ref}}) + 1 - \max(a_i^{\text{ref}})}{2} \\ &= \frac{1}{2} + \frac{\text{med}(a_i^{\text{ref}})}{2} \end{aligned} \tag{23}$$

where $\text{med}(a_i^{\text{ref}})$ is the fixed part of $a$ expressed from $V_{\text{med}}$ definition. As illustrated in Fig. 5, $\lambda_4$ is set between $\lambda_{4_{\text{high}}}$
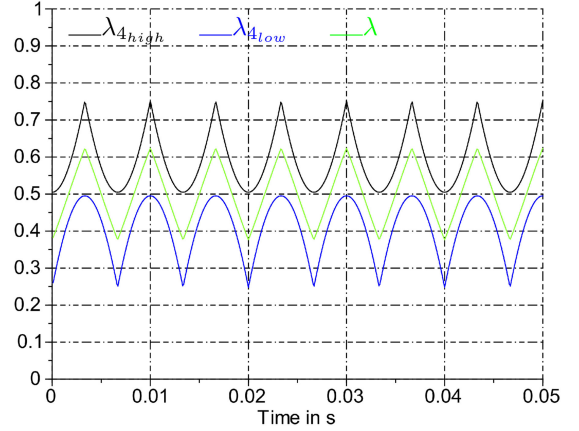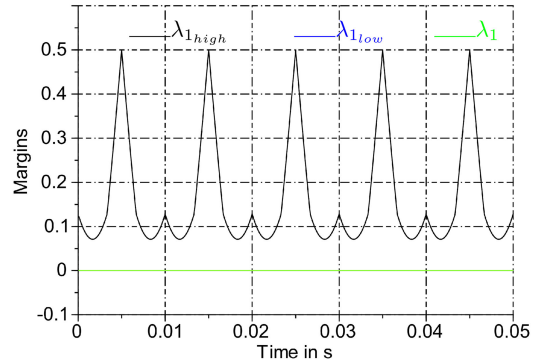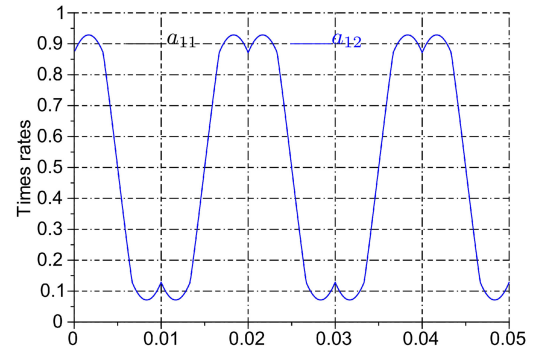


Fig. 5. $\lambda_4$ and its margins.



Fig. 6. $\lambda_i = 0$ $i \in \{1; 2; 3\}$, time rates, and bounds.

and $\lambda_{4_{\text{low}}}$. The relationship between (15) and (23) leads to the neutral point voltage

$$V_{no} = \frac{V_{\text{med}}}{2}. \tag{24}$$

### B. Per Leg Tuning Parameters

In this study, three $\lambda_i$ $i \in \{1, 2, 3\}$ are considered as follows.
1) $\lambda_i = 0$ defines $t_{i1} = t_{i2}$, leading to a two-switches leg inverter.
2) $\lambda_i = \lambda_{i_{\text{high}}}$ alternates between $t_{i1} = 0$ and $t_{i2} = T_{\text{sw}}$, leading to a reduction of the switching losses. Indeed, $K_{i1}$ or $K_{i3}$ are not switched for half a period, and $\frac{E}{2}$ edges on $V_{lo}$ are insured.
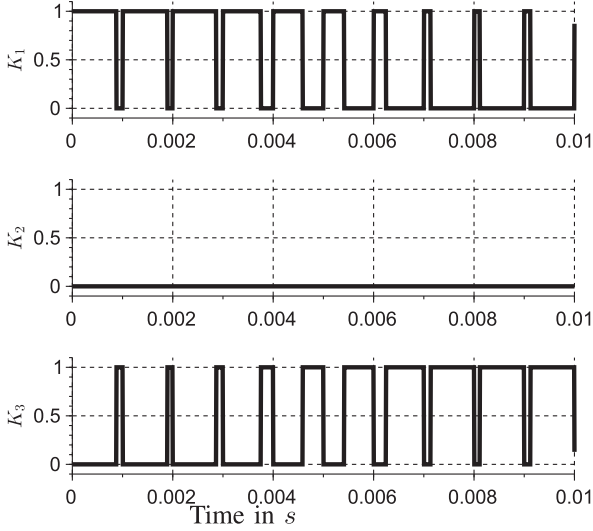
Fig. 7. $\lambda_i = 0$ switches sequence.

3) $\lambda_i = \frac{\lambda_{i\,\text{low}} + \lambda_{i\,\text{high}}}{2}$ maximizes the time between switching while all the switches are used during each switching period.

### C. Simulation

A Scilab [20] test-bench based on the switching cell given in Fig. 2 has been developed to test the three strategies proposed. The cell is connected to a $E = 50$-V dc bus. The switching frequency is set at $f_{\text{sw}} = 1$ kHz. The three modulation strategies have been tested by modulating 90% of a 25-Hz 50-V peak sinusoidal waveform.

The proposed strategies generate a signal, which fundamentally corresponds to the desired reference voltage.

*1) $\lambda_i = 0$:* This strategy introduces no shift between $a_{i1}$ and $a_{i2}$, as illustrated in Fig. 6. Consequently, the switch $K_{i2}$ is not used. As depicted in Fig. 7, the switching cell is working as a usual two-levels/two-switches cell. The voltages and switches states are plotted for half a period of the sine reference waveform. On one hand, $K_{i2}$ never switches, which reduces the number of switching, and consequently the switching losses, at each switching period. On the other hand, this strategy increases the harmonic distortion of the load current, due to a lower number of switching.

*2) $\lambda_i = \lambda_{i\,\text{high}}$:* This strategy introduces a difference between $a_{i1}$ and $a_{i2}$, as illustrated in Fig. 8. The three switches are thus used as displayed in Fig. 9. However, this figure points out that $K_{i2}$ is switched all along the period of $V_i^{\text{ref}}$, whereas $K_{i1}$ and $K_{i3}$ are used on half a period only. Such a strategy leads to clamp alternatively the time rates to 0 for $a_{i1}$, and 1 to $a_{i2}$. Indeed, $K_{i1}$ and $K_{i3}$ are only used, respectively, during the positive and negative parts of $V^{\text{ref}}$. Similarly to the previous strategy, the switching losses are reduced, but higher harmonic distortion will be experienced.

*3) $\lambda_i = \frac{\lambda_{i\,\text{low}} + \lambda_{i\,\text{high}}}{2}$:* This strategy involves all the switches of the cell at each switching period. As shown in Fig. 10, $a_{i1}$ and $a_{i2}$ are not set to 0 and 1, respectively, for more than one switching period. Thus, compared to the previous strategies, it leads
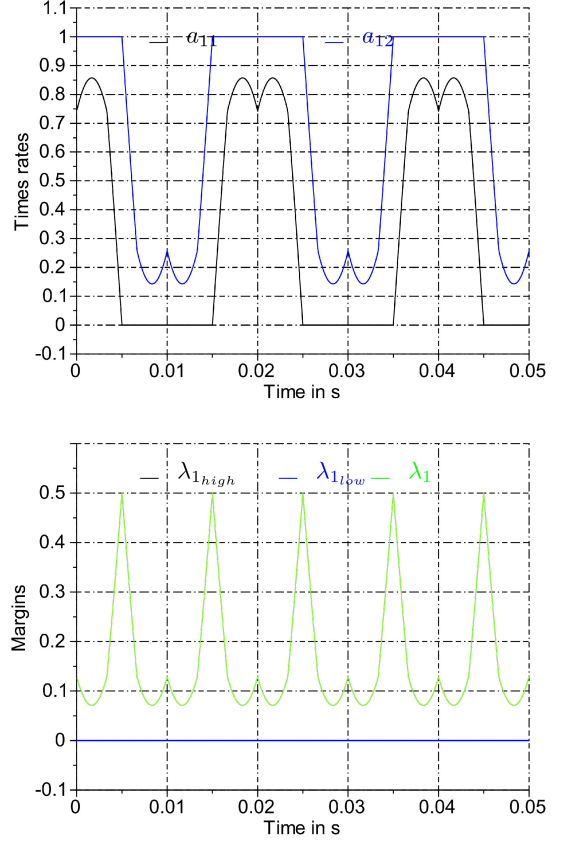


Fig. 8. $\lambda_i = \lambda_{i\,\text{high}}$ time rates and bounds.

to an increase of the switching losses. Three switching occur at each switching period, as illustrated Fig. 11. To conclude, these results highlight that the modeling scheme given in Fig. 4 is fulfilled.

## V. EXPERIMENTAL RESULTS

The three-phases inverter of the experimental test-bench is made up of three normal T-type switching cells modules, APTGLQ40HR120CT3G from Microsemi in Fig 12. A classical scheme will be used for the control/command layer: the command signals will be send to the switches trough a DSPACE device embedded with FPGA in order to format the signals (i.e., inclusion of the dead time). The signals applied are similar to those defined in Section IV-C. For every modulation strategy described above, the leg voltage $v_{lo}$ are displayed, as shown in Fig. 13.

### A. $\lambda_i = 0$

It is noticed that the high magnitude of the switching edges $\Delta v_{lo} = E$ seems to be an important factor, and also a drawback, concerning resonance phenomena as well as overall quality of currents.

### B. $\lambda_i = \lambda_{i\,\text{high}}$

Let us notice that this strategy does not suffer from the same drawback encountered in the previous strategy. Effectively, the
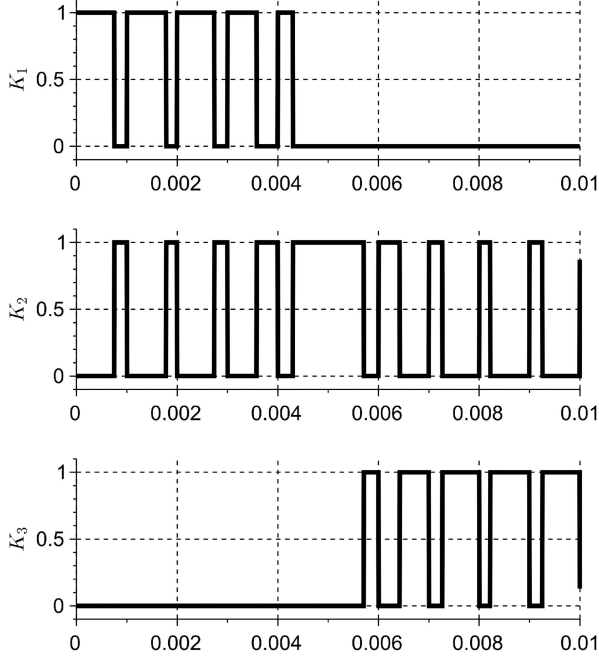
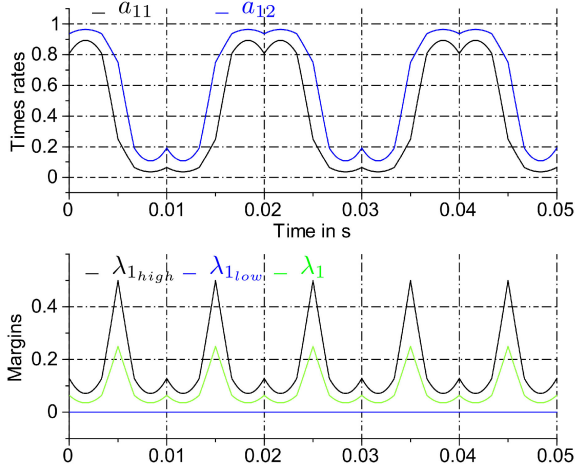Fig. 9. $\lambda_i = \lambda_{i_{\text{high}}}$ switches sequence.



Fig. 10. $\lambda_i = \frac{\lambda_{i_{\text{low}}} + \lambda_{i_{\text{high}}}}{2}$ time rates and bounds.

voltage edge is smaller

$$\Delta v_{lo} = \frac{E}{2}.$$

C. $\lambda_i = \frac{\lambda_{i_{\text{low}}} + \lambda_{i_{\text{high}}}}{2}$

A first advantage is to obtain a low distortion signal. Indeed, as displayed in Fig. 13, both $\Delta v_{lo} = E$ and $\Delta v_{lo} = E$ are encountered leading to mitigated voltage edges. Let us remark that the rising edges can be reduced by using a triangle carrier.

Consequently, it will produce only $\Delta v_{lo} = \frac{E}{2}$ voltage edges.

## VI. DISCUSSION

The main advantage of our contribution is to embed the design of modulation schemes in a generic framework. Indeed, the
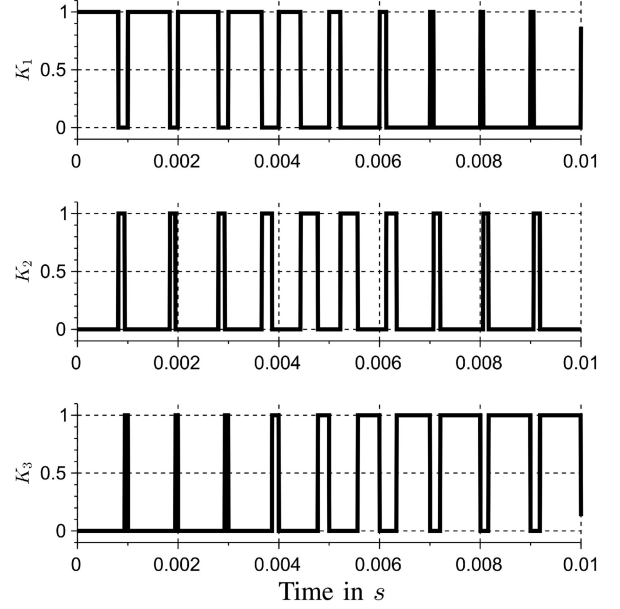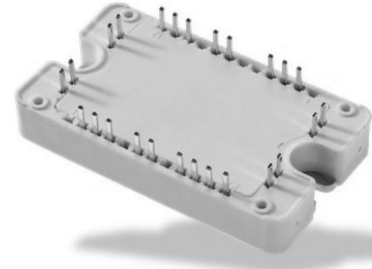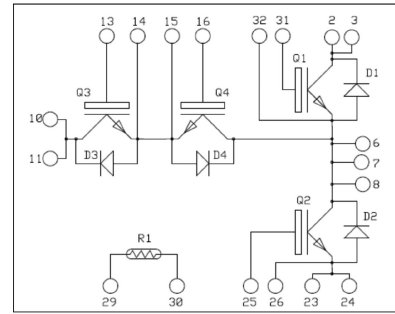


Fig. 11. $\lambda_i = \frac{\lambda_{i_{\text{low}}} + \lambda_{i_{\text{high}}}}{2}$ switches sequence.



(a)



(b)

Fig. 12. Microsemi T-type module. (a) Supplied module (b) Electrical scheme.

generic modeling process described in Section II can be used to any inverter topology. In addition, the modulation strategy definition in Section III is based on a generic mathematical tool. Moreover, software already provide stable algorithms for the calculus of our pseudoinverse matrices.

To highlight the efficiency of our method, we focus our discussion on the general solution provided in (13). The generic PWM scheme described is associated with the boundaries of the solution set. Indeed, free specific examples are illustrated. Following the criteria to optimize, power losses or voltage edges, for instance, one scheme must be applied. The modeling method
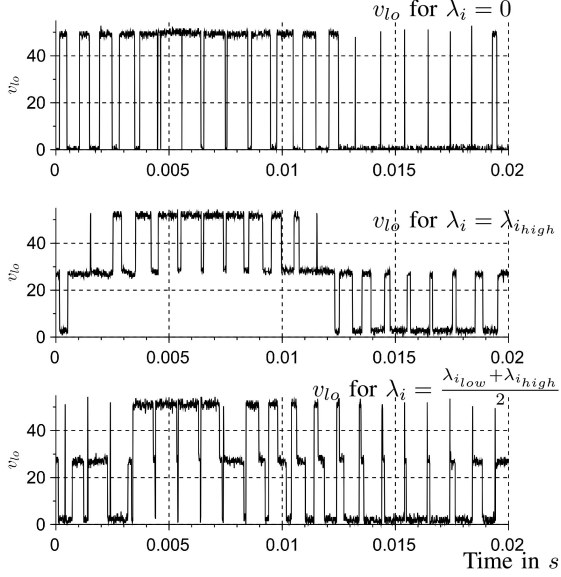
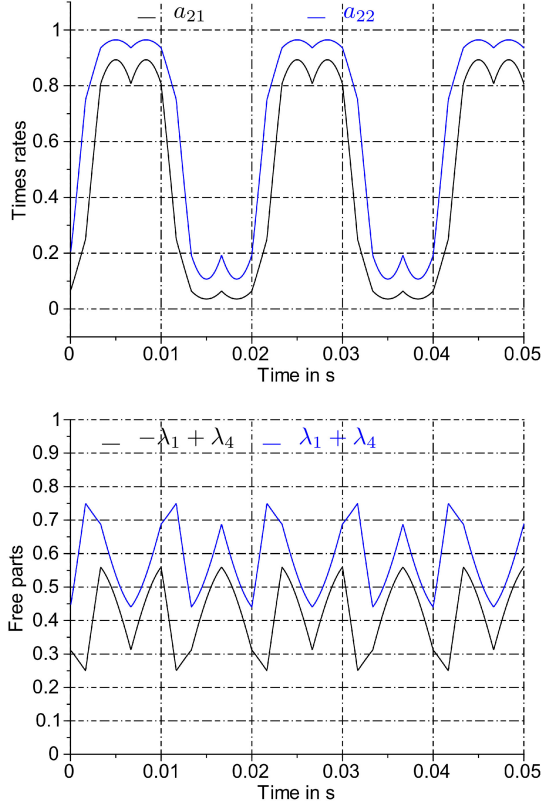Fig. 13. Output voltages $v_{lo}$ for the three described strategies.



Fig. 14. Independent part for time rates of the second leg.

allows us to implement a generic modulation scheme. Indeed, a simple *if* statement makes possible to switch at any time from one strategy to another one, where only the $\lambda_i$ $i \in 1, 2, 3$ will be changed. Moreover, it is highlighted that every expression can be defined, as it fits the maximal $\lambda_{i_{high}}$, an minimal 0, values. The nonlinear behavior of the system while functioning is not compromised. Effectively, the average model is only used to generate the time rate as references, before being com-

pared to a time representative signal. Finally, binary gate signals are generated.

More precisely in the solution expression (13), the fixed part, $(M \otimes A)^\dagger V^{\text{ref}}$ is directly computed from the desired reference voltages. It corresponds to averaged steady-state voltages. For every time rates $a_{ij}$, the independent part of the solution $F\lambda$ is made of the common component $\lambda_4$ and a per leg tuning parameter $\lambda_i$, $i \in \{1; 2; 3\}$. $\lambda_4$ was demonstrated to be proportional to the common mode voltage $v_{no}$ (24). Also, the proposed method exhibits easily the boundaries for the $\lambda_i$. It allows us to define immediately any expression for $\lambda_i$, which fulfills the constraints (22). For instance, when $\lambda_i = \frac{\lambda_{i_{low}} + \lambda_{i_{high}}}{2}$, $i \in \{1, 2, 3\}$, the time rates solution is obvious, whereas specific waveforms of the independent part $F\lambda$ are not. Indeed, based on the oneself-experience, it would have been difficult to suggest such a waveform, as displayed in Fig. 14.

As far as the method is concerned, it is pointed out that a single carrier is needed while all possible solutions are highlighted. Because the modulating signal obtained is consistent to a time rate, but also related to a switching time, it can be inserted into an SVM scheme. This is due to the fact that the modulation strategies modeling method is generic.

## VII. CONCLUSION

Based on a generic framework, the contribution exposed in this paper is twofold as follows.

1) A model of the T-type $3LT^2C$ converter is exhibited.
2) Control strategies for the T-type $3LT^2C$ are provided.

The mathematical model of the inverter considered paves the way to the modeling of any inverter topology.

Furthermore, the obtained model is a linear system easy to handle with mathematical linear system resolution techniques. This is used to involve the pseudoinverse theory when designing the control strategies. Such a tool is used to exhibit the degree of freedom of the linear solution set. The tuning parameters are then used to address the physical constraints of the inverter.

Simulation and experimental results have proven the feasibility of the proposed approach.

## APPENDIX
## MAXIMAL RANK FACTORIZATION

The independent solution is

$$I_6 - (M \otimes A)^\dagger (M \otimes A)z$$

$$= \frac{1}{6} \begin{bmatrix} 4 & -2 & 1 & 1 & 1 & 1 \\ -2 & 4 & 1 & 1 & 1 & 1 \\ 1 & 1 & 4 & -2 & 1 & 1 \\ 1 & 1 & -2 & 4 & 1 & 1 \\ 1 & 1 & 1 & 1 & 4 & -2 \\ 1 & 1 & 1 & 1 & -2 & 4 \end{bmatrix} z. \quad (25)$$

In such an expression, the components of $z$ are linked through the matrix $I_6 - (M \otimes A)^\dagger (M \otimes A)$. To highlight the four tuning parameters (11), a maximal rank factorization is performed.

$F_{6\times4}$ and $G_{4\times6}$ are defined so that $I_6 - (M \otimes A)^\dagger (M \otimes A)z = FGz = F\lambda$ where $\lambda$ components are the four tuning parameters.

$F$ is chosen to dispatch one tuning parameter per leg, and the last one is distributed over all the legs

$$F = \begin{bmatrix} -1 & 0 & 0 & 1 \\ 1 & 0 & 0 & 1 \\ 0 & -1 & 0 & 1 \\ 0 & 1 & 0 & 1 \\ 0 & 0 & -1 & 1 \\ 0 & 0 & 1 & 1 \end{bmatrix}.$$

## REFERENCES

[1] W. C. Rossmann and R. G. Ellis, "Retrofit of 22 pipeline pumping stations with 3000-hp motors and variable-frequency drives," *IEEE Trans. Ind. Appl.*, vol. 34, no. 1, pp. 178–186, Jan./Feb. 1998.

[2] R. Menz and F. Opprecht, "Replacement of a wound rotor motor with an adjustable speed drive for a 1400 kW kiln exhaust gas fan," in *Proc. 44th IEEE IAS Cement Ind. Tech. Conf.*, 2002, pp. 85–93.

[3] B. P. Schmitt and R. Sommer, "Retrofit of fixed speed induction motors with medium voltage drive converters using NPC three-level inverter high voltage IGBT based topology," in *Proc. IEEE Int. Symp. Ind. Electron.*, 2001, pp. 746–751.

[4] S. Bernert, "Recent developments of high power converters for industry and traction applications," *IEEE Trans. Power Electron.*, vol. 15, no. 6, pp. 1102–1117, Nov. 2000.

[5] S. Alepuz, S. Busquets-Monge, J. Bordonau, J. Gago, D. Gonzalez, and J. Balcells, "Interfacing renewable energy sources to the utility grid using a three-level inverter," *IEEE Trans. Ind. Electron.*, vol. 53, no. 5, pp. 1504–1511, Oct. 2006.

[6] J. Dixon, L. Moran, R. Rodriguez, and E. Domke, "Reactive power compensation technologies: State-of-the-art review," *Proc. IEEE*, vol. 93, no. 12, pp. 2144–2164, Dec. 2005.

[7] Y. Xuan, M. Tian, X. Song, W. Chen, and X. Yang, "Design and implementation of a high power three-level T-type inverter for a photovoltaic system," in *Proc. 9th Int. Conf. Power Electro.*, Seoul, South Korea, 2015, Jun. 1–5, pp. 2808–2813.

[8] M. Schweizer and J. W. Kolar, "High efficiency drive system with 3-level T-type inverter," in *Proc. 14th IEEE Int. Power Electron. Motion Control Conf.*, Birmingham, U.K., Aug. 30–Sep. 1, 2011, pp. 1–10.

[9] M. Schweizer and J. W. Kolar, "Design and implementation of a highly efficient three-level T-type converter for low-voltage applications," *IEEE Trans. Power Electron.*, vol. 28, no. 2, pp. 899–907, Feb. 2013.

[10] T. D. Nguyen, Q. D. Phan, N. D. Dao, and H. N. Nguyen, "The carrier-based PWM method to reduce common-mode voltage for three-level T-type neutral point clamp inverter," in *Proc. IEEE 9th Conf. Ind. Electron. Appl.*, 2014, pp. 1549–1554.

[11] U.-M. Choi, J.-S. Lee, and K.-B. Lee, "New modulation strategy to balance the neutral-point voltage for three-level neutral-clamped inverter systems," *IEEE Tran. Energy Convers.*, vol. 29, no. 1, pp. 91–100, Mar. 2014.

[12] P-E. Vidal, S. Cailhol, F. Rotella, K. Berkoune, A-M. Llor, and M. Fadel, "Generalized inverses applied to pulse width modulation for static conversion: A first study," in *Proc. Eur. Conf. Power Electron. Appl.*, Lille, France, 2013, pp. 1–10.

[13] H. Shin, K. Lee, J. Choi, S. Seo, and J. Lee, "Power loss comparison with different PWM methods for 3L-NPC inverter and 3L-T type inverter," in *Proc. Electron. Appl. Conf. Expo.*, 2014, pp. 1322–1327.

[14] N. Satheesh, "Advanced T-types NPC- 3 level modules: A new possibility with RB-IGBT's," in *Proc. Appl. Power Electron. Conf.*, 2014, pp. 21–24.

[15] A. Graham, *Kronecker Products and Matrix Calculus: With Applications.* Chichester, U.K.: Ellis Horwood, 1981.

[16] J. Brewer, "Kronecker products and matrix calculus in system theory," *IEEE Trans. Circuits and Syst.*, vol. CS-25, no. 9, pp. 772–781, Sep. 1978.

[17] C. F. Van Loan, "The ubiquitous Kronecker product," *J. Comput. Appl. Math.*, vol. 123, pp. 85–100, 2000.

[18] S. Cailhol, P.-E. Vidal, and F. Rotella, "A generic method of pulse width modulation applied to 3-level T-type NPC inverter," in *Proc. IEEE Int. Power Electron. Motion Control Conf.*, 2016, pp. 20–25, doi: 10.1109/EPEPEMC.2016.7751968.

[19] A. Ben-Israel and T. N. E. Greville, *Generalized Inverses: Theory and Applications*, 2nd ed. New York, NY, USA: Springer-Verlag, 2003.

[20] Scilab Enterprises, "Scilab: Logiciel open source gratuit de calcul numrique," Scilab Enterprises, Orsay, France, 2012. [Online]. Available: http://www.scilab.org.

**Simon Cailhol** received the Ph.D. degree from the Institut National Polytechnique de Toulouse, Toulouse, France, in 2015. His Ph.D. research concerned interactive path planning and virtual reality.

He started his research activity with an internship on power converters modelization and control in the Laplace Laboratory, Toulouse, France. From 2015, he was engaged with the LGP, ENIT, Universit de Toulouse, Toulouse, France, and changed his research topic to step back and focus on power electronics. He worked first on the multiphysics modelization of the materials of power electronics modules, from 2015 to 2016. From 2016, he works on the design of power converters for aeronautics.

**Paul-Etienne Vidal** received the Ph.D. degree from the Institut National Polytechnique de Toulouse, France, in 2004. He received the Habilitation à Diriger des Recherches in 2017.

From 2004 to 2006, he was a Temporary Researcher with the Laboratory LEEI, INP/CNRS. Since 2006, he is an Associate Professor with the Laboratoire Genie de Production, Toulouse University, Toulouse, France. His research interests include power converter efficiency. He developed three research themes within the PRIMES platform (http://www.primes-innovation.com/) facilities: electro- and thermo-mechanical modeling and simulations; experimental technology integration for power electronic device; and control strategy of power converters.

**Frédéric Rotella** (SM'96) was born in 1957. He received the Engineer Diploma from the Institut Industriel du Nord, Lille, France, in 1981, and the Doctor Engineering and Doctor of Physical Science degrees from the University of Science and Technology of Lille-Flandres-Artois, Lille, France, in 1983 and 1987, respectively.

From 1981 to 1994, he joined the Laboratoire d'Automatique et d'Informatique Industrielle de Lille where his research interests were focused on modelization, analysis, and control of nonlinear systems. During this period, he was with the École centrale de Lille (former Institut industriel du Nord) as an Assistant, from 1984 to 1989, and a Matîre de Conférences, in automatic control, from 1989 to 1994. In 1994, he joined the École nationale d'Ingénieurs de Tarbes (France), as a Professor in automatic control. He is currently with the Laboratoire de Génie de Production, École nationale d'Ingénieurs de Tarbes, France, where he is with the Research Team Decision, Interaction for Dynamical Systems. His research interests include observation for linear time-varying systems or nonlinear systems, and flatness-based control of nonlinear systems. He has authored or coauthored 40 technical papers and has also contributed to 13 edited books. Since 1990, he has coauthored eight French text books in automatic control and mathematics.